ChemCatChem

ChemCatChem
Chemistry Europe
European Chemical Societies Publishing

RESEARCH ARTICLE OPEN ACCESS

Temperature-Dependent Lithium Migration and Increased Thermal Stability Within Palladium Nanoparticles

Christopher Foo[1,2] | Ping-Luen Baron Ho[1] | Sarah Day[2] | Guangchao Li[3] | Shik Chi Edman Tsang[1]

[1]Wolfson Catalysis Centre, Department of Chemistry, University of Oxford, Oxford, UK | [2]Diamond Light Source, Harwell Science and Innovation Campus, UK | [3]Department of Applied Biology and Chemical Technology, The Hong Kong Polytechnic University, Hong Kong

Correspondence: Christopher Foo (chris.foo@diamond.ac.uk) | Guangchao Li (guangchao.li@polyu.edu.hk)

Received: 22 December 2025 | **Revised:** 20 January 2026 | **Accepted:** 20 January 2026

Keywords: light-element dopants | nanoparticle catalyst | palladium | synchrotron powder X-ray diffraction

ABSTRACT

The incorporation of light-element dopants into monometallic nanoparticle catalysts enables precise modulation of their electronic structures, thereby tailoring catalytic performance. However, despite the widespread use and general understanding of such systems, fundamental aspects of dopant–framework interactions and solid-solution behavior in light-element-doped metal nanoparticles remain incompletely characterized. Here, using a one-step synthesis of lithiated palladium (Pd) nanoparticles formed by an in situ lithiation process with lithium (Li) acetate, we investigate the temperature-dependent phase behavior of the Pd–Li solid solution by variable-temperature synchrotron powder X-ray diffraction (VT-SPXRD). In situ thermal Bragg diffraction studies reveal unexpected delithiation dynamics and phase complexity in the metastable PdLi intermetallic compound, including previously unreported temperature-dependent lithium migration and site-occupancy redistribution. Remarkably, we demonstrate that interstitial lithium doping enhances thermal stability from 150 °C to over 400 °C, with higher lithium loadings (0.5–1.5 eq) maintaining structural integrity up to 515 °C. This unexpected stabilization, attributed to nanoparticle encapsulation effects, provides fundamental insight into light-element doping mechanisms in metallic nanoparticles and paves the way for the rational design of electronically tuned nanocatalysts.

1 | Introduction

Palladium (Pd) -based materials are cornerstone catalysts in both homogeneous [1] and heterogeneous systems finding widespread application in hydrogenation, cross-coupling, electrocatalysis, and automotive emission control [2–9]. Extensive research has elucidated key structure–performance relationships in Pd catalysts, including the roles of lattice strain [6, 10], facet-dependence [11], size-dependence [12, 13], and nucleation [14, 15]. Interstitial atoms can be incorporated into the face-centered cubic (fcc, $Fm\bar{3}m$) Pd lattice to induce pronounced electronic perturbation with minimal atomic rearrangement, particularly light elements such as H, Li, B, and C. Interstitial B has been shown to enhance catalysis in formic acid oxidation [16], oxygen reduction [17], and partial hydrogenation of acetylene [4]. Interstitial C can be formed by ethylene hydrogenation [18, 19], glucose encapsulation [3, 5], and CO disproportionation [20]. Palladium hydride (PdH_x) is a well-researched compound with applications in hydrogen storage, purification, and sensing [14, 18, 21]. Despite these reports of emergent properties, the structural effects and stability remain significantly underexplored.

In particular, interstitial lithium doping in palladium remains virtually unexplored, despite its exceptional potential for strong

[†]Professor Shik Chi Edman Tsang deceased May 20, 2025

electronic modification. In our previous work, although neutral lithium metal (metallic radius ~167 pm) is too large to enter the fcc Pd lattice, Li^+ ions (ionic radius 76 pm) fit readily into octahedral voids, enabling the formation of metastable $PdLi_x$ solid solutions. Early high-temperature syntheses employing lithium acetate under inert atmosphere (550 °C, 1 bar Ar, 4 h) yielded topotactic interstitial doping with compositions stable under both ambient conditions and a range of catalytic environments [4]. Sakamoto et al. reported a room-temperature lithium solubility of ~4 mol%, increasing to a maximum of 10.3 mol% at higher temperature [22], consistent with a theoretical limit of ~0.1 electron transfer per Pd atom (i.e., 10 mol% octahedral occupancy) [23]. Our own prior work, employing total-scattering X-ray pair distribution function (XPDF) analysis, confirmed occupancies of up to 14 mol% in nanoparticles synthesized via reductive lithiation [4]. These discrepancies in reported lithium content highlight significant gaps in understanding the thermodynamic and kinetic factors governing lithium incorporation, site preference, and thermal stability in nanoscale palladium.

Interstitial doping offers a powerful yet subtle means of tailoring the d-band structure and chemisorption properties of palladium, often leading to enhanced activity, selectivity, or stability in catalytic transformations [24]. However, the resulting solid solutions are typically metastable at ambient temperature and prone to thermally induced dopant expulsion (deintercalation), which imposes strict limitations on synthesis, characterization, and practical deployment. Among light-element dopants in palladium, boron (B) is the most stable interstitial dopant (250 °C), followed by lithium (Li) (150–200 °C) [4], carbon (C) (150 °C) [25], then hydrogen (H) (135 °C) [26]. The limited thermal stability of interstitially doped palladium represents a critical barrier to industrial implementation. Most doped Pd systems undergo rapid delithiation/deintercalation above their characteristic temperatures, limiting their use in elevated-temperature catalytic processes. Understanding and enhancing the thermal stability of $PdLi_x$ is therefore essential for developing robust catalysts that maintain their electronic modifications under realistic operating conditions.

A critical challenge limiting the industrial implementation of Pd catalysts generally is thermal sintering, typically initiating above 300 °C and accelerating dramatically at higher temperatures, leading to loss of active surface area and catalytic deactivation [13]. Traditional approaches to prevent sintering include strong metal–support interactions, spatial confinement in porous materials, or encapsulation strategies, yet these often fail at temperatures above 500 °C or compromise catalytic accessibility. The development of inherently sinter-resistant Pd nanoparticles that maintain their nanoscale dimensions at elevated temperatures remains an unmet need for high-temperature catalytic applications.

In this work, we report a facile one-step synthesis of lithiated palladium nanoparticles ($PdLi_x$) via in situ reductive intercalation during solid-state nanoparticle formation, eliminating the need for post-synthetic or high-temperature doping protocols. The resulting metastable Pd–Li solid solution is subjected to detailed temperature-dependent structural analysis using variable-temperature synchrotron powder X-ray diffraction (VT-SPXRD). These experiments reveal complex and previously unobserved delithiation dynamics, including temperature-driven lithium migration between octahedral sites, partial site re-equilibration, and unexpected enhancement of thermal stability. This study provides the first view of Li dopant mobility and phase evolution in Pd nanocatalysts, establishing critical design rules for electronically modulated systems with improved robustness under operating conditions.

2 | Results and Discussion

2.1 | Post-Synthesis vs In Situ Lithiation of Pd Nanoparticles

A commercial monophasic, non-expanded 50 wt% Pd/C was post-synthesis lithiated by grinding with 0.35 eq of lithium acetate (LiOAc) precursor (an excess assuming 0.1–0.15 eq doping [4, 20, 22]) and heating at 250 °C for 12 h. Nanoparticle morphology was shown to be retained, well-distributing and lithium-doping to be successful by the contrast of TEM and EDX mapping (Figure 1a). The dominant Bragg product was the expanded PdLi at 98 wt%, while the non-expanded Pd phase was still present at 2% wt (Figure 1b). However, raising the reaction temperature to 350 °C significantly reduced the proportion of the expanded phase due to thermal instability of interstitial Li in Pd at > 300 °C, which has been proven in our group's previous work [4]. In contrast, using a large excess of lithium precursor (3.5 eq) achieved quantitative conversion to the expanded PdLi phase at both 250 °C and 350 °C. This demonstrates that a high Li chemical potential effectively stabilizes the doped lattice against thermal deintercalation, shifting the equilibrium toward higher lithium occupancy. Besides, their stability was probed by washing the materials with water to remove the surface LiOAc. The PdLi/C sample prepared at 350 °C with 3.5 eq precursor retained its expanded lattice parameter after washing, whereas the analogous material synthesized at 250 °C underwent rapid delithiation, reverting predominantly to the non-expanded Pd structure. These results indicate significantly stronger Li binding when doping is performed at 350 °C under Li-rich conditions.

To streamline catalyst preparation and enhance synthetic reproducibility, we developed a one-pot in situ protocol in which Pd nanoparticle nucleation, growth, and interstitial lithium incorporation occur concurrently. All samples below are synthesized using an in situ approach. Three lithium loadings were investigated: 0.20, 0.50, and 1.50 equivalents relative to Pd. STEM confirmed the expected nanoparticle morphology. SXPD revealed that even the lowest lithium loading (0.20 eq) yielded a dominant expanded fcc phase (PdLi) (Figure S1). This contrasts sharply with post-synthesis lithiation, where large precursor excesses (≥ 3.5 eq) were required for comparable phase purity. Thus, lithium incorporation during nanoparticle formation is more atom-efficient than post-synthesis lithiation, which requires slow diffusion of lithium from the surface into the bulk. Furthermore, the lithium-intercalation was shown to be stable to washing at a lower temperature: 250 °C rather than 350 °C (Figure 1b in pale). Nevertheless, complete elimination of the non-expanded Pd phase was not achieved; a minor residual fraction (4–7 wt%)

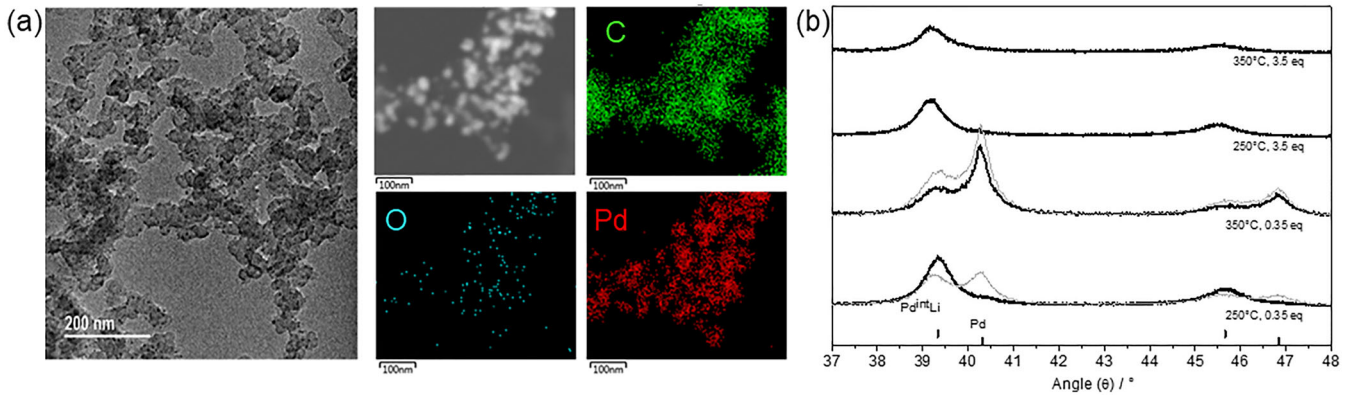

FIGURE 1 | (a) TEM micrographs and STEM EDX mapping of 50 wt% Pd post-synthesis doped with a large excess of lithium 0.35 eq at 250 °C for 12 h. The low concentration of oxygen shows that the Pd is in the desired reduced metallic form. EDX cannot map lithium. (b) Laboratory-source XRD showing the effect of temperature and lithium stoichiometry on post-synthesis lithium doping. Washed samples are shown in gray.

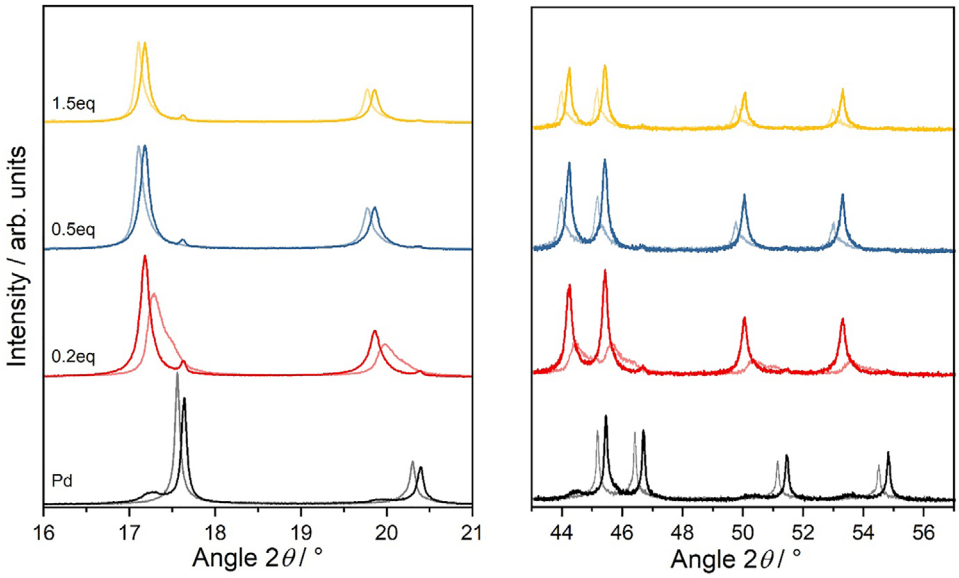

FIGURE 2 | SXPD of in situ lithiated 50 wt% PdLi/C: initial room temperature (thick line), final high temperature 550 °C (pale line).

persisted in all samples (Figure 2). This is tentatively attributed to thermodynamic and entropic contributions that favor a small population of Li-free domains under the dynamic conditions of particle formation.

Besides, for the post-synthesis method, increasing the Li:Pd ratio from 0.20 to 1.50 led to a progressive decrease in Bragg reflection intensity and slight peak broadening, despite near-constant phase composition of the expanded lattice (~94–96 wt%). This suggests that excess lithium induces local structural disorder, possibly through partial occupancy of tetrahedral sites, surface Li enrichment, or microstrain, without substantially altering long-range lattice expansion. These results demonstrate that, although bulk phase compositions appear similar, the in situ and post-synthesis PdLi materials are structurally and chemically distinct: the one-pot route offers superior lithium economy and simplified processing but introduces modest heterogeneity that may influence catalytic and delithiation behavior.

2.2 | Thermal Stability of In Situ Lithiated PdLi

The thermal stability of lithiated palladium nanoparticles represents a critical performance parameter for catalytic applications. To systematically evaluate this, we conducted VT-SXPD analysis from room temperature to 515 °C on samples using three lithium stoichiometries: 0.2, 0.5, and 1.5 eq (Figure 3). Initial room temperature characterization revealed similar Bragg diffraction patterns for all samples, with the expanded PdLi phase comprising 93–96 wt% and residual non-expanded Pd at 4–7 wt% (Figure 2). However, thermal treatment revealed dramatically different stability profiles dependent on lithium stoichiometry. Rietveld refinement was carried out for each dataset individually. For the 0.2, 0.5, and 1.5 eq datasets, the average Rwp = 8.737, 8.260, and 8.983, respectively, and the average GoF = 1.362, 1.223, and 1.129, respectively. Both the prolonged thermal stability and the unexpected intercalation are shown to be dependent on lithium doping (Figure 3). For the higher lithiation 0.5 eq/1.5 eq, $Pd^{int}Li$ remains above 93 wt% over the full temperature range

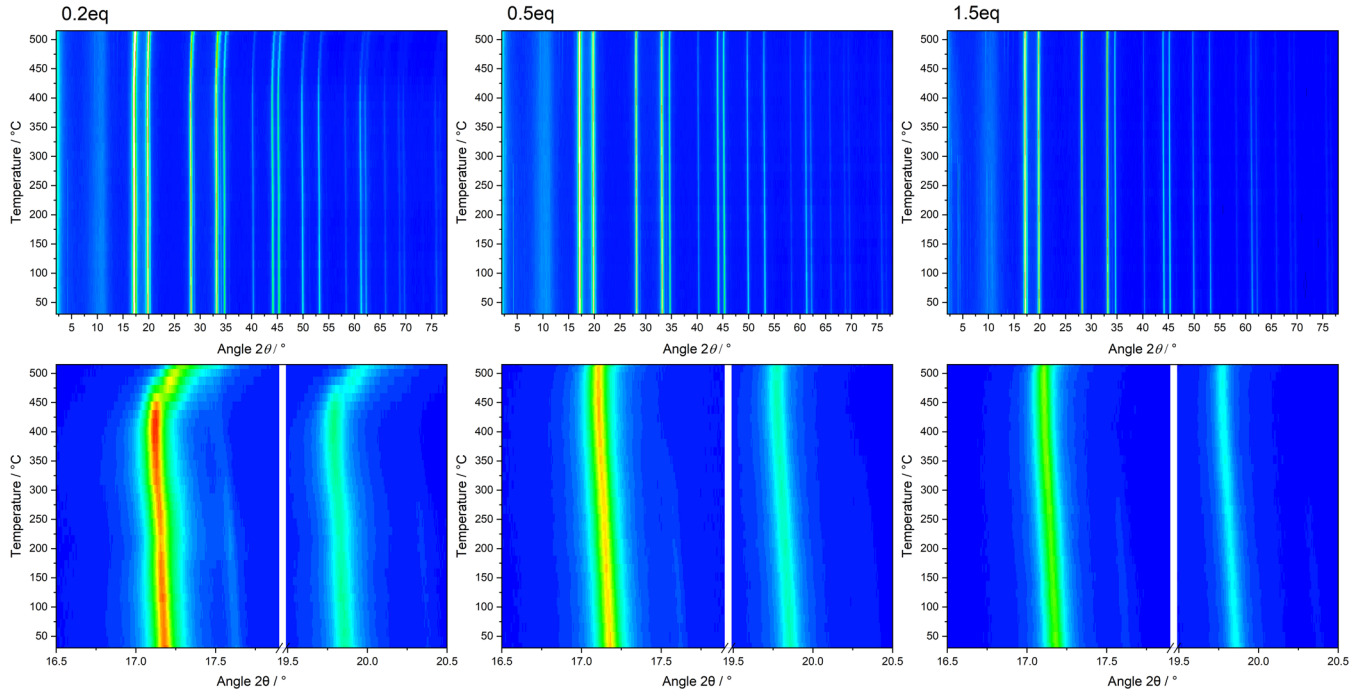

FIGURE 3 | VT-SXPD heatmaps of in situ lithiated 50 wt% PdLi/C showing (111) and (200) facets at 2θ angles of 17.2° and 19.8°, respectively, for (a) 0.2 eq, (b) 0.5 eq, and (c) 1.5 eq samples, showing the stability of the lithiated phase up to very high temperature.

up to 510 °C. Meanwhile for 0.2 eq, the PdintLi remains high (above 90 wt%) until above 400 °C, at which the phase splits into two phases, and the relative crystalline composition value is partitioned, causing peak overlap and poor peak resolution.

2.2.1 | Low-Temperature Regime (RT-150 °C): Thermal Expansion and Initial Stability

For all samples, up to 150 °C, the relative crystalline mass compositions remained stable (Figures 3 and 4a). The integrated intensities decrease approximately linearly with temperature caused by the increasing Debye–Waller factors (Figures 3 and 4b). Throughout this period of phase stability, the lattice parameters of Pd and $Pd^{int}Li$ increased approximately linearly (Figures 3 and 4c), consistent with standard thermal expansion for pristine palladium (Figure S2). This initial stability across all lithium loadings indicates that the interstitial lithium remains strongly bound within the octahedral sites at moderate temperatures.

2.2.2 | Intermediate Regime (150–400 °C): Occupancy Equilibration and Delta Lithiation

This temperature range reveals the most striking differences between samples and introduces novel phase behavior. For the lowest excess of precursor (0.2 eq), delithiation is observed at the expected temperature of 150–200 °C, shown by a decrease in the composition of $Pd^{int}Li$ (93–90 wt%) and a correlated increase in pristine Pd (Figure 4a). However, contrary to expectation, the delithiation was short-lived and did not continue to completion, with $Pd^{int}Li$ remaining highly stable at 200 °C. The lattice parameter evolution provides crucial mechanistic insights (Figure 4c). Similarly, between 150–200 °C, the $Pd^{int}Li$ phase showed evidence of deintercalation by the thermal expansion being countered by a compressive mechanism, resulting in an approximately constant lattice parameter. The partially delithiated phase is a labeled $PdLi_{x-\delta}$. The contraction is clear when the chemical effects of the dopant–framework interaction are separated from the thermal expansion by considering the thermal expansion of pristine Pd (Figure S2). Simultaneous to this delithiation of the PdLi in the 0.2 eq product, the pristine Pd phase expanded beyond thermal expansion predictions from 3.970 to 3.975 Å, yielding a partially expanded lithiated palladium phase $PdLi_{\delta}$. These negatively correlated phase behaviors in intensity and lattice parameter indicate lithium movement from $Pd^{int}Li$ to Pd (Equation 1), suggesting a closed system that retains lithium internally rather than losing it to the atmosphere. This internal lithium occupancy equilibration continued to 200 °C.

$$PdLi_x + Pd \rightarrow PdLi_{x-\delta} + PdLi_{\delta}$$

internal lithium occupancy equilibration (1)

Due to the solid–solution behavior of the system, the occupancy equilibration can be quantified using Vegard's law. At room temperature, the 93 wt% $PdLi_{0.15}$ and 7 wt% Pd equate to a total Vegard stoichiometry of $PdLi_{0.140}$. At the peak of the occupancy equilibration at 200 °C, there is 10 wt% $PdLi_{\delta}$ and 90 wt% $PdLi_{x-\delta}$, resulting in a total Vegard occupancy of $PdLi_{0.130}$. Most remarkably, at 200 °C, both intensity and lattice parameter trends reversed, indicating the reverse reaction, that is, lithiation of $PdLi_{x-\delta}$ by $PdLi_{\delta}$ (Equation 2), a phenomenon we term "delta lithiation".

$$PdLi_{x-\delta} + PdLi_{\delta} \rightarrow PdLi_x + Pd \quad \text{delta lithiation} \qquad (2)$$

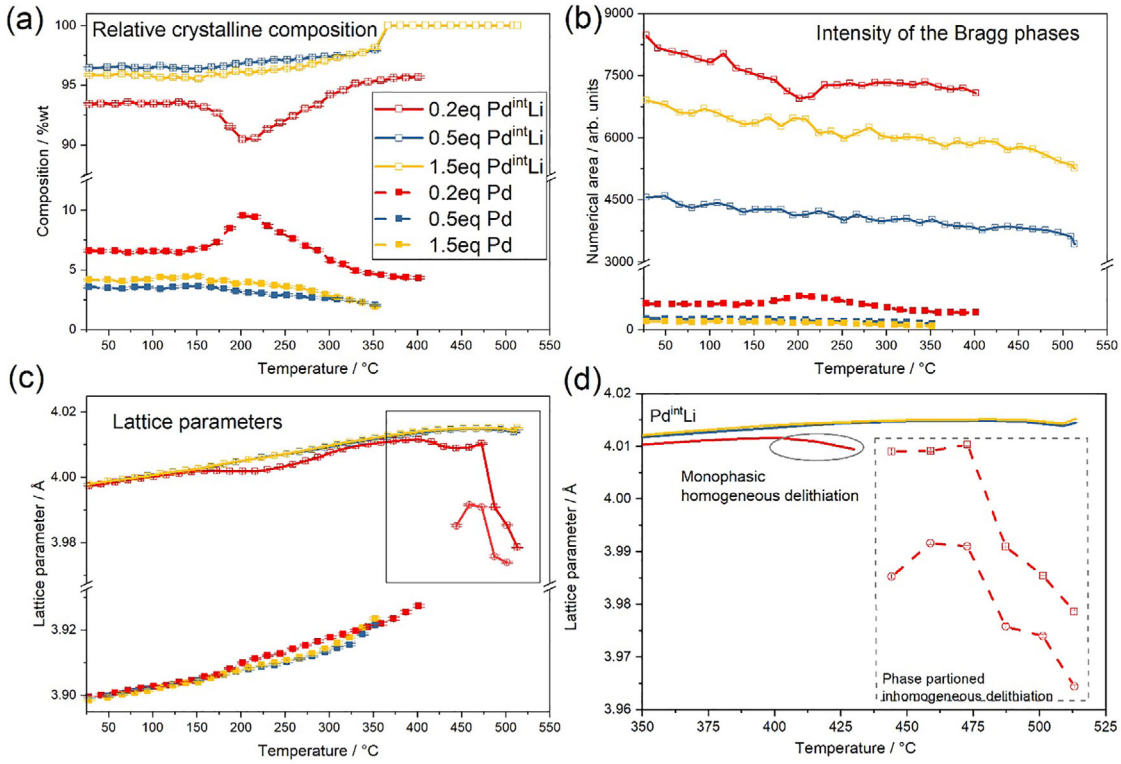

FIGURE 4 | Rietveld refinement of VT-SXPD for pristine and in situ lithiated Pd nanoparticles: Pd as dotted lines, PdLi as solid lines. (a) Relative crystalline composition, (b) integrated intensity of the Bragg phases, (c) lattice parameters, and (d) zoomed view of the box in (c) showing the detail of monophasic delithiation and phase partitioned delithiation.

This reverse reaction is highly unexpected as it works against entropic equilibration to form a higher energy doped product. As the $PdLi_{\delta}$ phase decreases, the high occupancy phase $PdLi_{x-\delta}$ remains approximately constant until 400°C, with increases counteracting the Debye–Waller effects. By 270°C, the total phase composition was restored to the initial room temperature values (93% Pd^{int}Li and 7% pristine Pd), though the $PdLi_x$ lattice parameter remained slightly expanded, indicating retained lithium or hysteresis effects. The total Vegard occupancy remained approximately unchanged at $PdLi_{0.136}$. The temperature-dependent reversibility of this lithium redistribution (Equations 1 and 2) likely reflects enthalpy–entropy compensation effects. At lower temperatures (150–200°C), the entropic driving force favors lithium equilibration across available sites, resulting in the formation of PdLiδ at the expense of the high-occupancy phase. However, as temperature increases to 200°C and above, enthalpic contributions—potentially including lattice strain relief in the high-occupancy phase or strengthening of Pd–Li interactions at elevated temperature—become increasingly favorable, driving the reverse reaction. This creates the unexpected 'delta lithiation' where the system reorganizes to restore the thermodynamically preferred high-occupancy configuration.

Critically, samples synthesized using higher lithium loadings (0.5 and 1.5 eq) exhibited fundamentally different behavior—they showed no occupancy equilibration at 150°C or delta lithiation at 200 °C at any temperature. Instead, both pristine and lithiated Pd phases increased linearly in lattice parameter with thermal expansion and decreased linearly in intensity by Debye–Waller effects throughout the 150–325 °C range. This loading-dependent behavior demonstrates that these novel phase transitions require specific structural conditions present only at lower lithium contents. We propose that the sharp threshold between 0.2 and 0.5 eq represents a percolation limit: at 0.2 eq, sufficient vacant octahedral sites and structural flexibility enable lithium mobility between phases, whereas at 0.5–1.5 eq, the extensively modified lattice creates kinetic barriers through increased site–site interactions and reduced available diffusion pathways. At higher loadings, lithium atoms are more densely packed in the interstitial sublattice, potentially creating cooperative effects that kinetically trap the system in its initial configuration despite thermodynamic driving forces for redistribution.

2.2.3 | High-Temperature Regime (>400 °C): Enhanced Stability and Phase Partitioning

The greatest effect of lithium excess was observed in high-temperature phase stability. The pristine Pd phase became increasingly unstable at higher lithium loadings, disappearing at 400 °C, 380 °C, and 365 °C for 0.2, 0.5, and 1.5 eq, respectively (Table 1). However, no correlated increase in PdLi intensity or lattice parameter change was observed, suggesting formation of an amorphous lithium–palladium product caused by a closed, volume-restricted system. It is highly surprising to observe the disappearance of the low occupancy palladium (<3.93 Å) before the expanded phase (>3.99 Å), and importantly, crystalline pristine Pd never reforms even after high-temperature treatment to 515 °C. In conventional delithiation processes, the bulk fcc Pd structure is restored. Instead, we observe only partially

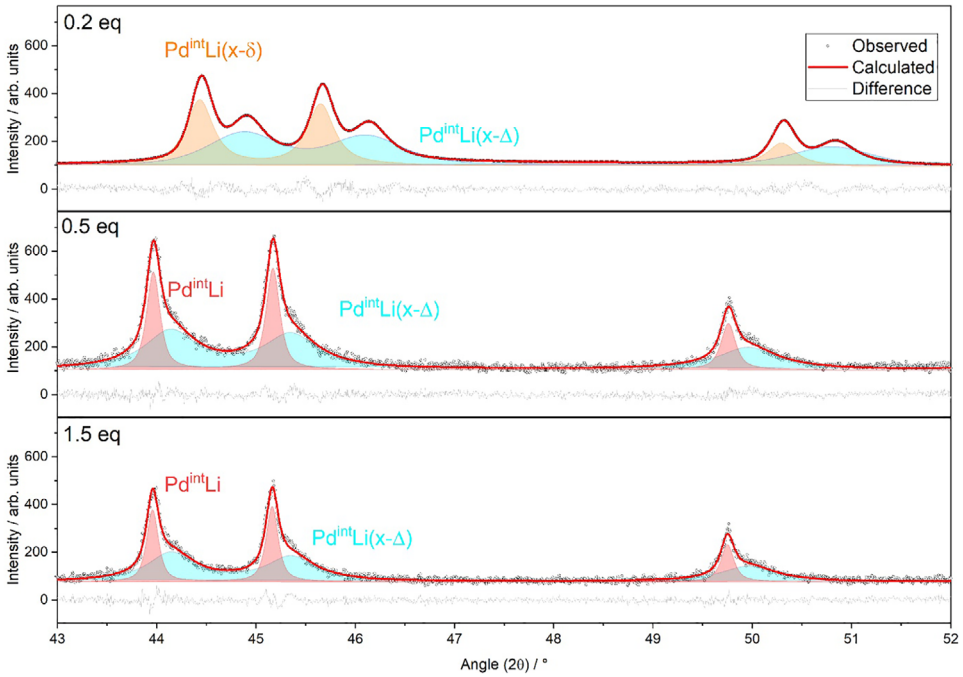

FIGURE 5 | Rietveld fitting of SXPD patterns at 515 °C showing phase partitioning of the high occupancy expanded phase, exemplified by greater separation at high-angle: (331), (420), (422), and (511).

TABLE 1 | Temperature range of thermal instability of Pd and PdLi (first observation of decreasing intensity to complete disappearance) at various lithium doping levels by VT-SXPD.

Lithium precursor/eq	Pd/°C	PdLi/°C
0.2	345–400	415->515
0.5	150-380	480->515
1.5	150-365	480->515

contracted phases (3.959–3.980 Å at 515 °C) with significant peak broadening. We propose that lithium does exit the system through oxidative delithiation, but the delithiation process creates a highly defective, strained, or partially amorphous Pd product rather than well-ordered crystalline palladium. This could arise from: (i) kinetically trapped structural distortions created during lithium extraction, (ii) high densities of vacancies, dislocations, or stacking faults that disrupt long-range order, or (iii) very small crystallites where surface disorder dominates the XRD signal. This is also supported by the broadening of the $PdLi_{x-\delta}$ phases. The absence of the characteristic pristine Pd reflection throughout the entire temperature range represents a significant departure from conventional delithiation behavior and warrants further investigation.

For the 0.2 eq sample, the expanded PdLi phase eventually decomposed starting at 415 °C. This delithiation proved non-homogeneous, with the phase splitting into two distinct populations with different lattice parameters from ~430 °C, which is observed very clearly as peak splitting (Figure S4 for direct visualization of this partitioning behavior of (235) and (411)): 4.01 Å (86 wt%) and 3.99 Å (14 wt%) (Figures 4d and 5). This phase partitioning, not previously reported, indicates varying delithiation rates within the sample. Both phases continued contracting to 515 °C, reaching 3.980 Å ($PdLi_{0.010}$, 52 wt%) and 3.959 Å ($PdLi_{0.078}$, 48 wt%), with significant peak broadening suggesting highly disordered transitions. The heterogeneous nature of this delithiation, rather than a uniform lattice contraction, likely arises from multiple factors. First, smaller nanoparticles may result in more rapid delithiation. TEM analysis (Figures 1a and S1) confirms a distribution of particle sizes (5–15 nm), which would naturally lead to a distribution of delithiation rates. Second, local compositional variation may arise from either the original synthesis or the lithium redistribution described above. This heterogeneity could create domains with different initial lithium occupancies that respond differently to thermal treatment. The observation that phase partitioning occurs at different temperatures depending on lithium loading (460 °C for 0.2 eq vs. 515 °C for 0.5 and 1.5 eq) supports the hypothesis that initial lithium concentration and local structural environment are critical factors governing the onset and progression of heterogeneous delithiation. The higher lithium excess samples (0.5 and 1.5 eq) exhibited remarkable $Pd^{int}Li$ stability, showing only minor intensity decreases at 480 °C and maintaining >90% of initial intensity at 515 °C despite Debye–Waller effects. At 480 °C, a small contraction indicates homogenous delithiation (Figure 4d). Then, in only the final patterns at 515 °C, the phase partitions to a minor contracted phase (3.99 Å) (Figure 5), similar to the 0.2 eq sample but occurring at much higher temperature. As this was the final temperature surveyed, the contraction was not observed to completion. For no sample is there observation of the return of crystalline pristine Pd.

Delithiation processes in all samples are shown to occur at much higher temperatures and over a much wider range than conventionally observed. Additionally, thermally unstable weak unindexed low-angle reflections around 4° (~9.2 Å) decomposed

above 300 °C for all lithiated samples (Figure S3), while very weak unidentified high-temperature byproducts emerged from ~450 °C (Figure S5), suggesting complex lithium chemistry at elevated temperatures. Notably, the peak broadening of delithiated phases at elevated temperatures indicates the absence of particle sintering, which would typically manifest as peak narrowing due to increased crystallite size. This broadening instead suggests increased structural disorder or strain, consistent with a system under confinement that prevents the particle migration and coalescence characteristic of sintering processes.

2.3 | Discussion of Unexpected Thermal Stability

The exceptional thermal stability observed in our in situ lithiated Pd nanoparticles—particularly at higher lithium loadings—demands a mechanistic explanation. Traditional PdLi materials decompose rapidly above 150–200 °C through oxidative delithiation when exposed to air. Our observations of stability extending to 480–515 °C represent a paradigm shift in understanding these materials. We propose a multi-factor stabilization mechanism. First, a kinetic stabilization through physical encapsulation. The in situ synthesis appears to create a protective barrier around the nanoparticles, likely carbonaceous in nature [5, 27], that limits oxygen access. This is evidenced by the closed-system behavior during lithium redistribution in the 0.2 eq sample, where total lithium content remained constant despite phase changes. Examples are known of designed encapsulation in order to decrease deactivation and sintering, and increase size selectivity, conductivity, and yield [27–29]. In many cases, these encapsulated materials are used in LIB as enhanced-performance electrode materials [29, 30].

Another mechanism is evidenced by the 0.5 and 1.5 eq samples, which show fundamentally different behavior, suggesting that higher lithium occupancy creates a more thermodynamically stable interstitial configuration. The absence of any lithium migration below 480 °C indicates stronger Pd–Li binding at these compositions. Direct experimental verification of these hypotheses would benefit from complementary lithium-sensitive techniques in future works, such as ^{7}Li solid-state NMR. The enhanced thermal stability demonstrated in this work opens opportunities for employing electronically modified palladium catalysts in high-temperature processes that were previously inaccessible to doped systems. Specific reaction classes operating at 300–500 °C that could benefit include catalytic combustion of methane and volatile organic compounds (VOCs) for emission control [31], and steam reforming of alcohols (methanol, ethanol) and light hydrocarbons for hydrogen production [32]. In many catalytic processes electronic modification of Pd could enhance low-temperature performance and improve resistance to poisoning and sintering.

The unexpected lithiation of pristine Pd phases at high temperature, drawing lithium from PdLi, demonstrates that the system maintains a stable lithium reservoir, since lithium acetate is no longer present, having been combusted during the synthesis process, and is not observed by XRD. It may seem feasible that carbon from the support is being doped into the Pd, but this has never been observed, and we have shown in this report that carbon is unstable in the Pd lattice in air above 150 °C. This internal reservoir effect is more pronounced at higher initial lithium loadings, explaining the enhanced stability. The phase partitioning observed above 400 °C provides additional insights. Rather than uniform delithiation, the system segregates into lithium-rich and lithium-poor domains, suggesting that lithium diffusion becomes the rate-limiting step at high temperatures. This heterogeneous decomposition pathway differs markedly from the homogeneous delithiation typically observed in post-synthesis doped materials. The possibility of retaining the lithium dopant and associated chemical enhancements for catalysis, while increasing thermal stability is an exciting prospect.

3 | Conclusions

This study elucidates the complex phase behavior of palladium nanoparticles during thermal lithiation and delithiation, establishing clear relationships between synthetic conditions, interstitial atom incorporation, and thermal stability. We demonstrate that in situ lithiation during nanoparticle synthesis not only provides a more atom-efficient route to PdLi but also fundamentally alters the material's thermal properties. Most significantly, interstitial lithium dramatically enhances thermal stability from the typical 150–200 °C limit to over 480 °C for samples with 0.5–1.5 eq lithium loading, representing a transformative improvement that enables high-temperature catalytic applications previously inaccessible to electronically modified palladium. The discovery of reversible lithium migration between phases, including the unexpected delta lithiation phenomenon at intermediate temperatures, reveals these systems to be far more dynamic than previously understood through behavior that appears to be governed by enthalpy–entropy compensation effects and percolation thresholds in the interstitial sublattice. The observation that delithiation produces structurally disordered Pd rather than recovering the pristine bulk lattice reveals fundamental differences between nanoparticulate and bulk delithiation mechanisms, with implications for understanding dopant dynamics in nanoscale materials. Importantly, the materials demonstrate resistance to crystallite size increase even at 515 °C, addressing one of the primary failure mechanisms in high-temperature catalytic applications. The strong dependence of thermal behavior on initial lithium loading, with a critical threshold between 0.2 and 0.5 equivalents, indicates that dopant concentration controls not just electronic properties but also fundamental stability mechanisms. These findings establish new design principles for light-element doped nanocatalysts and warrant further investigation into the nature of the proposed encapsulation effects and the broader applicability of this synthetic approach to other metal–dopant systems.

4 | Experimental Section

4.1 | Materials

Carbon-black (Vulcan XC72R GP-3921, particle size: 50 nm) was purchased from CABOT. Graphite, palladium acetate ($Pd(OAc)_2$), ethanol, lithium acetate dihydrate ($Li(OAc)_2H_2O$ were purchased from Sigma-Aldrich. All materials were used as received unless otherwise stated.

4.2 | Palladium Nanoparticle Synthesis

The procedure established by Chen et al.[25] was adapted to yield high palladium loading carbon black. Typically, a target palladium loading of 50% wt was used. Carbon black (200 mg) and $Pd(OAc)_2$ (169 mg) were ground until homogeneous, then decanted into an alumina crucible, and placed in a quartz-tube furnace. The system was purged with argon at 500 cm^3 min^{-1} for at least 15 min. Under continuous argon flow, the reaction was heated to 550 °C at 10 °C min^{-1}, held for 4 h, before being allowed to cool to room temperature. The temperature, heating rate, and hold duration were varied during the investigation, and will be referred to by the notation: temperature/rate/hold-time. Palladium supported on carbon black is referred to as Pd/cb, and palladium supported on graphite as Pd/gr. A separate one-step in situ lithiation was carried out by including $Li(OAc)_2H_2O$ in the nanoparticle formation step.

4.3 | One-Step In Situ Lithiated Palladium Nanoparticle Synthesis

A one-step in situ lithiation was carried out by including $Li(OAc).H_2O$ in the carbon black and $Pd(OAc)_2$ reaction mixture. Li:Pd stoichiometries of 0.2, 0.5, and 1.5 eq were used. The mixture was ground until homogeneous, then decanted into an alumina crucible, and placed in a quartz-tube furnace. The system was purged with argon at 500 cm^3 min^{-1} for at least 15 min. Under continuous argon flow, the reaction was heated to 350 °C at 10 °C min^{-1}, held for 12 h, before being allowed to cool to room temperature.

4.4 | Variable-Temperature Synchrotron X-Ray Powder Diffraction

Thermal stability was monitored by VT-SXPD at BL02b2, SPring-8. Wavelength and zero-error were refined to 0.689556 Å and -0.00015°, respectively. Non-doped and in situ lithiated 0.2, 0.5, and 1.5 eq samples were scanned from room temperature to 515 °C at 15 °C intervals. The temperature readout was accurate to ± 0.05 °C. Hence, over the three samples, the sampled temperatures are not coincident but highly accurate, but often deviate from the input temperature. Temperatures were rounded to the nearest 5 °C to establish an equivalence between the datasets.

4.5 | TEM

The samples were dispersed using 1 mg of sample in approximately 1 mL of dry ethanol. The mixture was sonicated for 30 min to form a uniform suspension. One drop of the suspension on a Holey carbon film 400 copper mesh grid forms a dispersed film less than 200 nm thick, and dried in the air prior to analysis. Finally, the copper sample grid was transferred to a JEOL ARM-200F for measurement. The following parameters were used: probe current of 80 pA, a semi-convergence angle of 23–25 mrad, and an accelerating voltage of 200 kV. The microscope was aligned before every experiment by using a gold standard sample ensuring 0.08 nm resolution under normal conditions. EDX was carried out using a Centurion spectrometer. EELS was carried out on a Gatan GIF Quantum 965 ER with an energy resolution of 0.9 eV, a beam diameter of approximately 100 nm, and a semi-collection angle of ~2.5 mrad. Data processing of EELs spectra included pre-edge background subtraction, removal of plural scattering by Fourier-ratio deconvolution, and normalization by integration of the post-edge intensity.

Acknowledgments

The support for this project from the EPSRC in the United Kingdom (Grant EP/K040375/1), The Hong Kong Polytechnic University (PolyU P0055278, P0055259, P0058122), the Department of Science and Technology of Guangdong Province (GDSTC 2025A1515011688), the Hong Kong Research Grants Council (15301725), the Shenzhen Science and Technology Program (JCYJ20250604185422030), and the National Natural Science Foundation of China (W2541007) are gratefully acknowledged. SXPD at BL02B2(2022B0539, 2021B1623), SPring-8 was assisted by Shogo Kawaguchi.

Conflicts of Interest

The authors declare no conflicts of interest.

Data Availability Statement

The authors declare that the data supporting the findings of this study are available within the paper and its supplementary information files. All relevant data are available from the authors.

References

1. T. Iwasawa, M. Tokunaga, Y. Obora, and Y. Tsuji, "Homogeneous Palladium Catalyst Suppressing Pd Black Formation in Air Oxidation of Alcohols," *Journal of the American Chemical Society* 126 (2004): 6554–6555.

2. C. Evangelisti, N. Panziera, P. Pertici, et al., "Palladium Nanoparticles Supported on Polyvinylpyridine: Catalytic ActiVity in Heck-Type Reactions and XPS Structural Studies," *Journal of Catalysis* 262 (2009): 287–293.

3. C. W. A. Chan, A. H. Mahadi, M. M.-J. Li, et al., "Interstitial Modification of Palladium Nanoparticles With Boron Atoms as a Green Catalyst for Selective Hydrogenation," *Nature Communications* 5 (2014): 5787.

4. I. T. Ellis, E. H. Wolf, G. Jones, et al., "Lithium and Boron as Interstitial Palladium Dopants for Catalytic Partial Hydrogenation of Acetylene," *Chemical Communications* 53 (2017): 601–604.

5. C. W. A. Chan, K. Y. Tam, J. Cookson, P. Bishop, and S. C. Tsang, "Palladium with Interstitial Carbon Atoms as a Catalyst for Ultraselective Hydrogenation in the Liquid Phase," *Catalysis Science & Technology* 1 (2011): 1584–1592.

6. J.-Y. Lin, C. Xi, Z. Li, et al., "Lattice-Strained Palladium Nanoparticles as Active Catalysts for the Oxygen Reduction Reaction," *Chemical Communications* 55 (2019): 3121–3123.

7. A. L. Bugaev, A. A. Guda, I. A. Pankin, et al., "Operando X-ray Absorption Spectra and Mass Spectrometry Data During Hydrogenation of Ethylene Over Palladium Nanoparticles," *Data in Brief* 24 (2019): 103954.

8. F. R. Fortea-Pérez, M. Mon, J. Ferrando-Soria, et al., "The MOF-Driven Synthesis of Supported Palladium Clusters With Catalytic Activity for Carbene-Mediated Chemistry," *Nature Materials* 16 (2017): 760–766.

9. Y. Ishikawa, S. Kimura, K. Takase, et al., "Modulation of Benzene or Naphthalene Binding to Palladium Cluster Sites by the Backside-Ligand Effect," *Angewandte Chemie* 127 (2015): 2512–2516.

10. A. Ulvestad, M. J. Welland, S. S. E. Collins, et al., "Avalanching Strain Dynamics During the Hydriding Phase Transformation in Individual Palladium Nanoparticles," *Nature Communications* 6 (2015): 10092.

11. K. Sytwu, F. Hayee, T. C. Narayan, A. L. Koh, R. Sinclair, and J. A. Dionne, "Visualizing Facet-Dependent Hydrogenation Dynamics in Individual Palladium Nanoparticles," *Nano Letters* 18 (2018): 5357–5363.

12. H. Akiba, M. Kofu, H. Kobayashi, et al., "Nanometer-Size Effect on Hydrogen Sites in Palladium Lattice," *Journal of the American Chemical Society* 138 (2016): 10238–10243.

13. V. V. Srabionyan, A. L. Bugaev, V. V. Pryadchenko, L. A. Avakyan, J. A. Bokhoven, and L. A. Bugaev, "EXAFS Study of Size Dependence of Atomic Structure in Palladium Nanoparticles," *Journal of Physics and Chemistry of Solids* 75 (2014): 470–476.

14. Z. Zhao, X. Huang, M. Li, et al., "Synthesis of Stable Shape-Controlled Catalytically Active β-Palladium Hydride," *Journal of the American Chemical Society* 137 (2015): 15672–15675.

15. S. Z. Mortazavi, P. Parvin, A. Reyhani, A. N. Golikand, and S. Mirershadi, "Effect of Laser Wavelength at IR (1064 nm) and UV (193 nm) on the Structural Formation of Palladium Nanoparticles in Deionized Water," *The Journal of Physical Chemistry C* 115 (2011): 5049–5057.

16. H. Wang, X. Qian, S. Liu, et al., "Boron-Doped PdCuAu Nanospine Assembly as an Efficient Electrocatalyst Toward Formic Acid Oxidation," *Chemistry—A European Journal* 26 (2020): 2493–2498.

17. J. Li, J. Chen, Q. Wang, W.-B. Cai, and S. Chen, "Controllable Increase of Boron Content in B-Pd Interstitial Nanoalloy to Boost the Oxygen Reduction Activity of Palladium," *Chemistry of Materials* 29 (2017): 10060–10067.

18. A. L. Bugaev, O. A. Usoltsev, A. A. Guda, et al., "Palladium Carbide and Hydride Formation in the Bulk and at the Surface of Palladium Nanoparticles," *The Journal of Physical Chemistry C* 122 (2018): 12029–12037.

19. A. L. Bugaev, A. A. Guda, I. A. Pankin, et al., "The Role of Palladium Carbides in the Catalytic Hydrogenation of Ethylene Over Supported Palladium Nanoparticles," *Catalysis Today* 336 (2019): 40–44.

20. M. Maciejewski and A. Baiker, "Incorporation of Carbon Into Palladium During Low-temperature Disproportionation of Carbon Monoxide Over Palladium/Zirconia Prepared From Gl Assy Palladium-Zirconium," *The Journal of Physical Chemistry* 98 (1994): 285–290.

21. A. L. Bugaev, A. A. Guda, A. Lazzarini, et al., "In Situ Formation of Hydrides and Carbides in Palladium Catalyst: When XANES is Better Than EXAFS and XRD," *Catalysis Today* 283 (2017): 119–126.

22. Y. Sakamoto, F. L. Chen, J. Muto, and T. B. Flanagan, "Phase Transitions in the Palladium-Rich Pd—Li Alloy System and Hydrogen Solubility in the Solid Solution Alloys," *Zeitschrift für Physikalische Chemie* 173 (1991): 235–250.

23. C. D. Gelatt, A. R. Williams, and V. L. Moruzzi, "Theory of Bonding of Transition Metals to Nontransition Metals," *Physical Review B* 27 (1983): 2005–2013.

24. T. Chen, C. Foo, and S. C. E. Tsang, "Interstitial and Substitutional Light Elements in Transition Metals for Heterogeneous Catalysis," *Chemical Science* 12 (2021): 517–532.

25. S. B. Ziemecki, G. A. Jones, D. G. Swartzfager, R. L. Harlow, and J. Faber, "Formation of Interstitial Palladium–Carbon Phase by Interaction of Ethylene, Acetylene, and Carbon Monoxide With Palladium," *Journal of the American Chemical Society* 107 (1985): 4547–4548.

26. L. E. A. Berlouis, P. J. Hall, A. J. MacKinnon, et al., "The Decomposition of Electrochemically Loaded Palladium Hydride: A the Rmal Analysis Study," *Journal of Alloys and Compounds* 253-254 (1997): 207–209.

27. D. Xu, H. Lv, and B. Liu, "Encapsulation of Metal Nanoparticle Catalysts Within Mesoporous Zeolites and Their Enhanced Catalytic Performances: A Review," *Frontiers in Chemistry* 6 (2018): 550.

28. H. O. Otor, J. B. Steiner, C. García-Sancho, and A. C. Alba-Rubio, "Encapsulation Methods for Control of Catalyst Deactivation: A Review," *ACS Catalysis* 10 (2020): 7630–7656.

29. G. Cui, Y.-S. Hu, L. Zhi, et al., "A One-Step Approach Towards Carbon-Encapsulated Hollow Tin Nanoparticles and Their Application in Lithium Batteries," *SmallSmall* 3 (2007): 2066–2069.

30. Y. Yu, L. Gu, C. Zhu, P. A. Aken, and J. Maier, "Tin Nanoparticles Encapsulated in Porous Multichannel Carbon Microtubes: Preparation by Single-Nozzle Electrospinning and Application as Anode Material for High-Performance Li-Based Batteries," *Journal of the American Chemical Society* 131 (2009): 15984–15985.

31. F. Kong, B. Nie, L. Jiang, et al., "Progress in Palladium-Based Bimetallic Catalysts for Lean Methane Combustion: Towards Harsh Industrial Applications," *The Innovation Materials* 3 (2025): 100116.

32. M. Zhang, D. Liu, Y. Wang, et al., "Recent Advances in Methanol Steam Reforming Catalysts for Hydrogen Production," *CatalystsCatalysts* 15 (2025): 36.

Supporting Information

Additional supporting information can be found online in the Supporting Information section.

Supporting File: cctc70587-sup-0001-SuppMat.docx.